

# Light-Directed Particle Patterning by Evaporative Optical Marangoni Assembly

Subramanyan Namboodiri Varanakkottu,<sup>†,‡,§,||</sup> Manos Anyfantakis,<sup>†,‡,§,||</sup> Mathieu Morel,<sup>†,‡,§</sup> Sergii Rudiuk,<sup>†,‡,§</sup> and Damien Baigl<sup>\*,†,‡,§</sup>

<sup>†</sup> Department of Chemistry, Ecole Normale Supérieure-PSL Research University, 24 rue Lhomond, F-75005, Paris, France

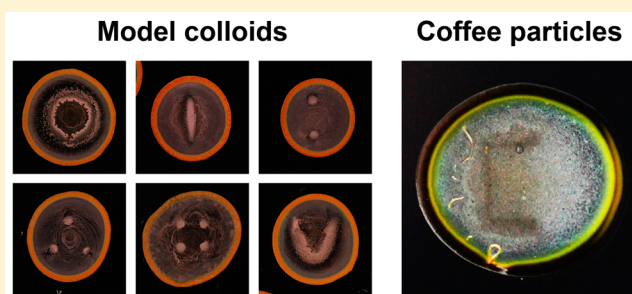
<sup>‡</sup> UPMC Univ Paris 06, PASTEUR, Sorbonne Universités, F-75005, Paris, France

<sup>§</sup> UMR 8640 PASTEUR, CNRS, F-75005, Paris, France

## Supporting Information

**ABSTRACT:** Controlled particle deposition on surfaces is crucial for both exploiting collective properties of particles and their integration into devices. Most available methods depend on intrinsic properties of either the substrate or the particles to be deposited making them difficult to apply to complex, naturally occurring or industrial formulations. Here we describe a new strategy to pattern particles from an evaporating drop, regardless of inherent particle characteristics and suspension composition. We use light to generate Marangoni surface stresses resulting in flow patterns that accumulate particles at predefined positions. Using projected images, we generate a broad variety of complex patterns, including multiple spots, lines and letters. Strikingly, this method, which we call evaporative optical Marangoni assembly (eOMA), allows us to pattern particles regardless of their size or surface properties, in model suspensions as well as in complex, real-world formulations such as commercial coffee.

**KEYWORDS:** Particle patterning, evaporation, directed assembly, photocontrol, Marangoni flow



Precise control over the organization of nano- and microparticles on solid surfaces is an important challenge for the successful integration of particles into devices as well as for the exploitation of specific properties emerging from their collective behavior.<sup>1–5</sup> Directed self-assembly strategies exploiting convective<sup>6</sup> and capillary<sup>7,8</sup> effects are powerful methods to organize particles on surfaces.<sup>9</sup> However, with these methods, patterned substrates are required to direct particle organization on the substrate, offering exquisite control down to single-particle resolution<sup>10</sup> but hindering any reconfigurability for a given substrate. Using an external light stimulus instead of inherent topological features appears as an interesting alternative offering enhanced flexibility, high spatiotemporal resolution and the possibility to use various kinds of substrates. The majority of photocontrolled methods have been focused on light-triggered control of particle aggregation, mainly in bulk or gel phases<sup>11,12</sup> and occasionally on solid substrates,<sup>13,14</sup> through light-sensitive particle–particle or particle–interface interactions. These surface chemistry-based methods pose the problem of applicability to arbitrary particle systems or complex formulations found in everyday life or in industry. Here we propose to exploit flows, rather than particle–particle or particle–substrate interactions, to manipulate particles regardless of their specific features (charge, size, etc.) and use light to guide their deposition into arbitrary predefined patterns from evaporating drops.

Mainly two possibilities to generate light-controllable flows inside a sessile drop can be envisioned. The first one consists in using a laser that locally heats the drop<sup>15,16</sup> to generate anisotropic evaporation profiles,<sup>17</sup> cavitation bubbles,<sup>18</sup> electrokinetic effects,<sup>19</sup> or thermocapillary stresses.<sup>20,21</sup> Less sensitive to the chemical nature of the particles to be patterned than the photochemical strategies described above, these temperature-based approaches require a fine yet challenging control over the temperature profile inside the sample drop, making them poorly suited for broad applicability or realization of well-defined complex patterns. Here, we propose an isothermal, straightforward yet powerful alternative to optically deposit particles at predefined positions. It consists in dissolving photosensitive surfactants in the suspension drop and use light patterns to generate photochemical surface tension-driven interfacial flows, which we call optical Marangoni flows.

When a pinned sessile drop dries on a substrate, an evaporation-driven flow toward the contact line accumulates particles there leading, after drop drying, to a typical ring-shaped deposit.<sup>22</sup> Most research efforts have been devoted to the suppression of this so-called coffee-ring effect.<sup>23–25</sup> For instance, we have recently shown that adding a very specific

**Received:** October 28, 2015

**Revised:** November 26, 2015

**Published:** December 2, 2015

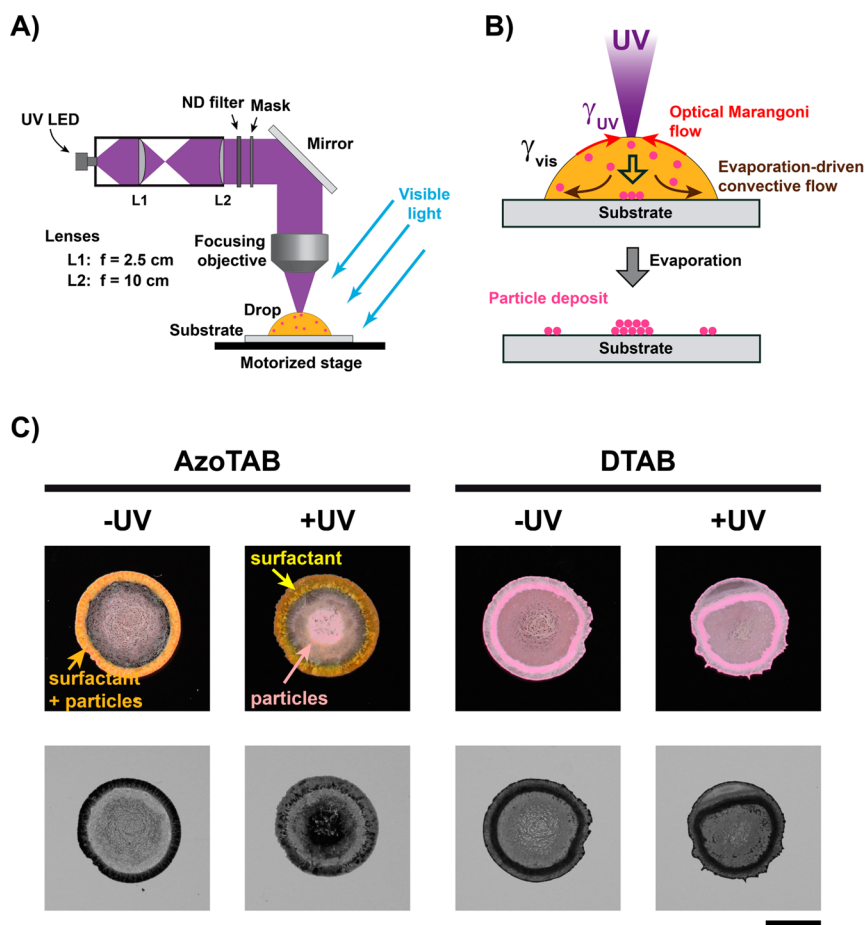


**Figure 1.** Light-directed particle deposition by evaporative optical Marangoni assembly. (A) Experimental setup: a sessile colloidal suspension drop is evaporating while being illuminated by a 370 nm UV pattern (focused spot or projected image using a mask) under homogeneous white light. (B) In the presence of AzoTAB photosensitive surfactant, the water/air surface tension is higher under UV ( $\gamma_{UV}$ ) than under visible light ( $\gamma_{VIS}$ ) thus creating optical Marangoni flows, which, combined with the evaporation-driven convective flow, deposit particles at specific positions. (C) Real-color reflection images (top) and black-and-white transmission images (bottom) of deposits obtained from a 7  $\mu\text{L}$  suspension drop (red-fluorescent carboxylate polystyrene particles, 1.1  $\mu\text{m}$  diameter, 2  $\text{mg}\cdot\text{mL}^{-1}$ ) with AzoTAB (10 mM) or with the nonphotosensitive analog DTAB (10 mM), without (–UV) or with (+UV) the application of UV during evaporation. Scale bar is 2 mm.

amount of oppositely charge surfactants corresponding to particle neutralization led to particle trapping at the liquid/gas interface and homogenization of the deposit pattern.<sup>26</sup> Using photosensitive surfactant led to the photocontrol of this process.<sup>27</sup> However, all of these methods led to final patterns with a more or less pronounced ring- or disk-shaped morphology, making impossible any fine intradrop particle patterning. Here, with the objective to precisely pattern particles rather than suppressing the coffee-ring effect, we used photosensitive surfactants at high concentrations to be in a regime where particles carry either their bare charge (like-charged systems) or are overcharged by surfactant adsorption (oppositely charged systems), thus hindering the possibility of interfacial trapping. We used light to generate internal flows directing the deposition of particles regardless of their charge and of solution composition, which enabled us to create arbitrary patterns of various kinds of particles from model suspensions to real-world formulations.

Figure 1 shows our concept and experimental setup to achieve evaporative optical Marangoni assembly (eOMA). We used AzoTAB (Supporting Information, Figure S1), a photosensitive surfactant known to induce an increase of the water/air surface tension ( $\gamma$ ) upon UV illumination ( $\gamma_{UV}$ ), which can

be reversibly switched upon visible illumination to a lower value ( $\gamma_{VIS}$ ).<sup>28–30</sup> The resulting surface tension difference  $\Delta\gamma = \gamma_{UV} - \gamma_{VIS}$  of the order of a few  $\text{mN}\cdot\text{m}^{-1}$ , is sufficient to generate  $\text{mm}\cdot\text{s}^{-1}$  to  $\text{cm}\cdot\text{s}^{-1}$  optical Marangoni flows at the water/air interface.<sup>31–33</sup> A  $\mu\text{L}$ -sized aqueous colloidal suspension drop containing AzoTAB was deposited on a glass substrate. AzoTAB concentration was chosen to be larger than regimes where particle–water/air interface interactions dominate<sup>26,27</sup> and slightly below the critical micellar concentration (CMC = 12.6 mM and 14.6 mM for *trans*- and *cis*-AzoTAB, respectively<sup>34</sup>). All experiments shown herein have been performed with a fixed AzoTAB concentration (10 mM) but experiments at a slightly lower concentration (7.5 mM) showed similar performance. White light was applied evenly on the drop and a custom-built optical setup was used to produce a UV light pattern at the drop surface (Figure 1A). This allowed us to maintain a surface tension pattern at the free interface with local maxima of  $\gamma$  located in the UV-exposed area. The drop was protected from ambient air flows and we let it evaporate under controlled temperature ( $22.5 \pm 1$  °C) and humidity ( $45 \pm 10\%$ ) conditions. In this configuration, the drop volume was subjected to mainly two types of flows: the evaporation-driven radial flow, known to transport particles

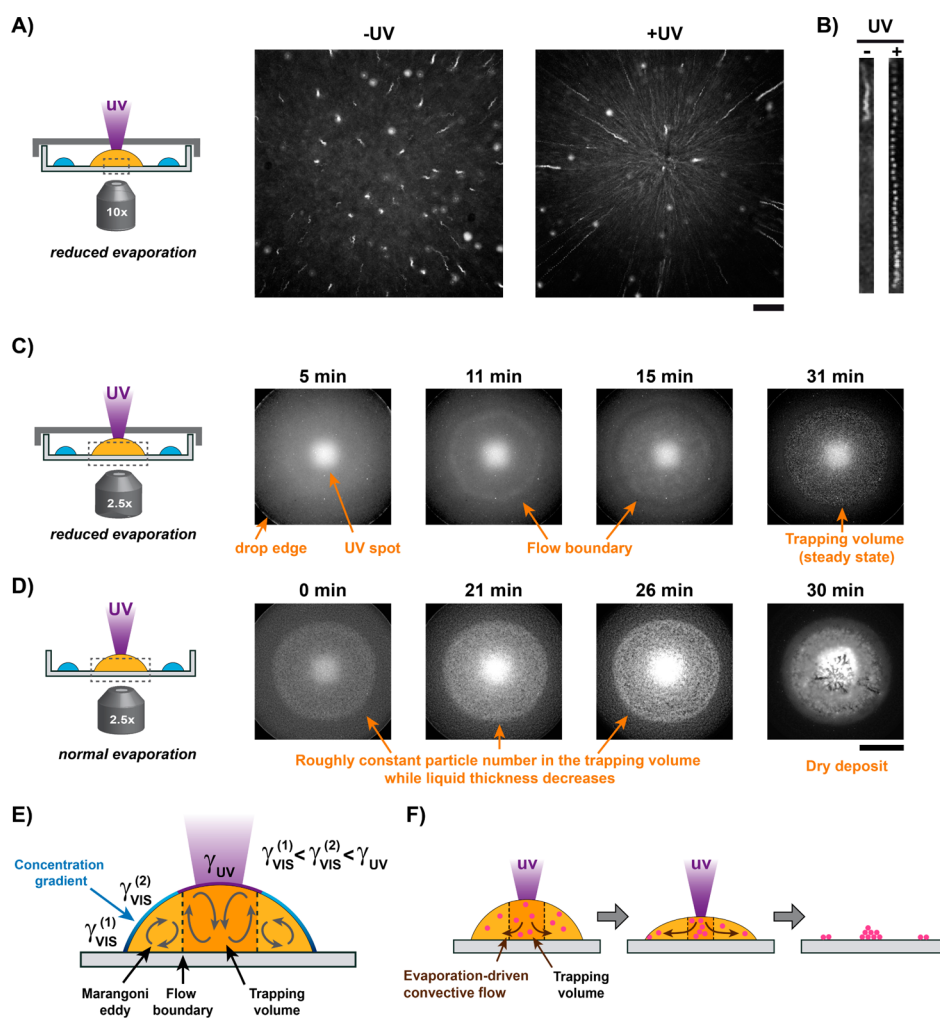


**Figure 2.** Light-induced flow pattern controls particle deposition. (A) High-magnification fluorescence streak velocimetry image without (left) or with (right) UV illumination (focused spot) at the drop surface under reduced evaporation conditions using a cover and water drops placed around a  $5 \mu\text{L}$  colloidal suspension drop (same composition as in Figure 1) with AzoTAB (10 mM). The focal plane for imaging is just above the substrate in the center of the drop (dashed box). Each image is a maximum intensity superposition of 144 images taken every 5 s. Scale bar is  $100 \mu\text{m}$ . (B) Streak velocimetry tracking of a single particle (or particle aggregate) during 195 s at approximately the same distance from the center. Each image is  $16 \mu\text{m} \times 253 \mu\text{m}$ . (C, D) Low-magnification fluorescence time lapse microscopy of the suspension drop under UV spot illumination under reduced evaporation conditions (C) followed by normal evaporation after cover removal (D). Scale bar is 1 mm. (E) Marangoni eddies at the edge due to AzoTAB concentration gradient toward the contact line and light-induced Marangoni flows pointing toward UV light create a volume where particles are trapped, defined by the boundary between the two circulating flows. (F) During evaporation, the convective flow transports particles toward the edge while the trapping volume shrinks and accumulates particles in the illuminated area, resulting in light-controlled particle deposition.

toward the drop contact line,<sup>22,35</sup> and circulating flows induced by the optical Marangoni stresses at the drop surface pointing toward each local maximum of  $\gamma$ . We hypothesized that the combination of these two effects would generate a flow pattern that could specifically deposit particles at the UV spot positions (Figure 1B). We first used an anionic particle suspension (red-fluorescent carboxylate polystyrene particles,  $1.1 \mu\text{m}$  diameter,  $2 \text{ mg}\cdot\text{mL}^{-1}$ ) and characterized the effect of a single circular UV light spot ( $500 \mu\text{m}$  diameter,  $1.0 \times 10^3 \text{ W}\cdot\text{m}^{-2}$ ) on the deposit morphology after drop drying. Photographs taken in reflection and transmission mode show that, without UV, AzoTAB (yellow color in reflection mode) and most particles (pink color) formed a typical ring-shaped pattern due to the evaporation-driven flow accumulating them at the contact line (Figure 1C left). Note that a small amount of particles were present inside the ring, attributed to the AzoTAB concentration gradient at the contact line, which could induce a small recirculating Marangoni flow toward the drop center. A similar

phenomenon was observed with dodecyltrimethylammonium bromide (DTAB, Figure 1C right), a nonphotosensitive analog of AzoTAB (same cationic polar headgroup, similar hydrophobic hydrocarbon tail,  $\text{CMC} = 13.4 \text{ mM}$ <sup>36</sup>), confirming the role of surfactants in creating Marangoni flows that partially redistribute particles during drop drying.<sup>37</sup> Interestingly, the application of UV dramatically affected the particle deposition behavior in the presence of AzoTAB. In this case, most particles accumulated at the center of the deposit rather than at its edge, where AzoTAB was still mainly present (note that more significant deposition of AzoTAB in the center can occur if a much larger concentration is used). When DTAB was used instead of AzoTAB, UV had no effect on particle deposition, showing that light-directed particle deposition in AzoTAB-laden suspensions was driven by UV-induced surface tension changes at the drop surface. These results show for the first time that UV light can direct particle deposition at a specific position during the evaporation of a colloidal sessile drop, with

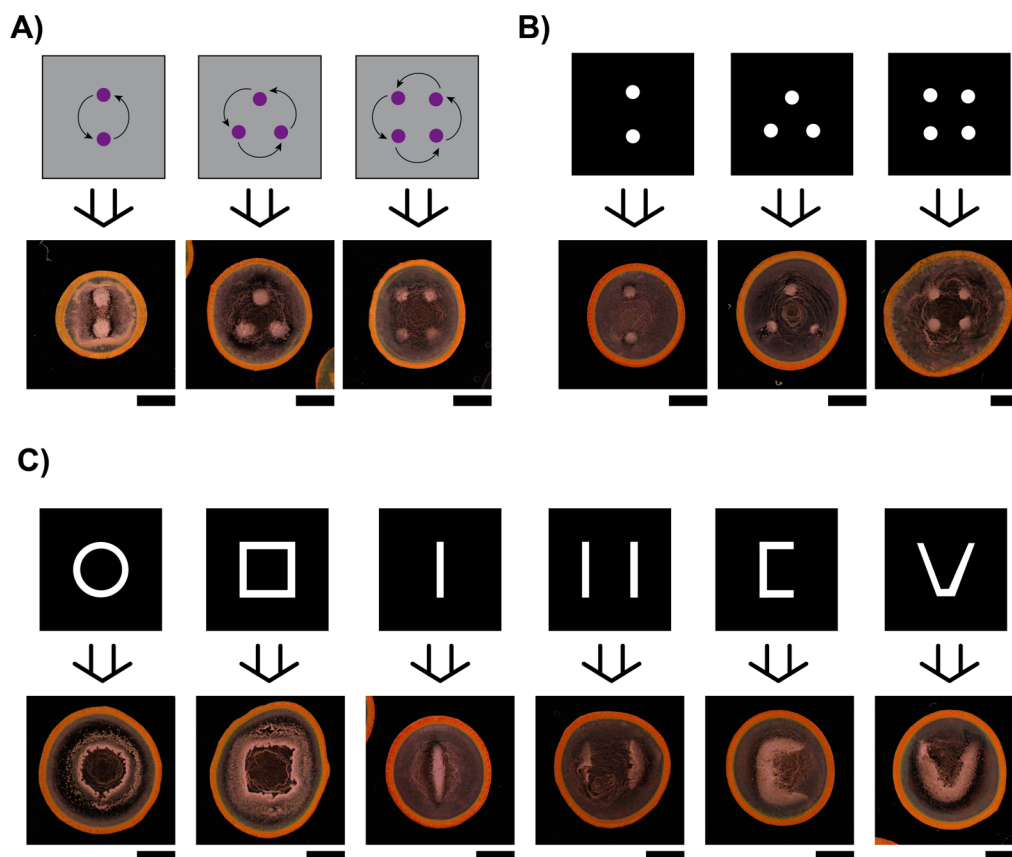


**Figure 3.** Complex particle patterning. (A–C) Real color reflection images of deposits obtained by UV illumination of a colloidal suspension drop (same composition as in Figure 1) with AzoTAB (10 mM). Multispots (A, B) and complex patterns (C) are obtained using single spot scanning (A) or an image projected on the drop surface through a photomask (B, C). The spot scanning pathway or the photomask is displayed above each deposit image. The drop volume was 12  $\mu\text{L}$  (A) or 15  $\mu\text{L}$  (B, C) except for the upper right pattern (20  $\mu\text{L}$ ). All scale bars are 2 mm.

the only requirement being the addition of a photosensitive surfactant to the suspension. This method is highly robust as the same behavior was reproducibly observed for various drop volumes (5 to 20  $\mu\text{L}$ ) and particle concentrations (0.2 to 5  $\text{mg}\cdot\text{mL}^{-1}$ ), as long as the drop remained pinned on the substrate. Note that depinning occasionally occurred in our system, especially for the lower particle concentrations, resulting in perturbations of the deposit morphology by the contact line motion. Moreover, since no specific particle–substrate interaction was necessary for this patterning process, it was possible to recover surfactant and/or particles upon adequate rinsing of the deposit with pure water.

To get insight into the light-driven deposition mechanism, we analyzed the particle motion during drop evaporation (Figure 2). First, to extract the component due to the Marangoni flows, we strongly reduced the evaporation-driven flow by placing the drop in a closed chamber with a nearly saturated atmosphere. High-magnification, streak velocimetry images in the vicinity of the substrate at the center of the drop showed that, without UV, particles were mainly diffusing but displayed also a slow converging motion toward the substrate, denoting a recirculating flow attributed to concentration gradient-induced Marangoni flows at the drop surface (Figure 2A, left, and Supporting Information, Movie S1). When a UV spot was applied at the center of the drop, the converging motion of particles was strongly enhanced (Figure 2A, right, and Supporting Information, Movie S2) with the radial velocity of particles (projected on the imaging focal plane) increasing

from 0.3  $\mu\text{m}\cdot\text{s}^{-1}$  ( $-UV$ ) to 1.2  $\mu\text{m}\cdot\text{s}^{-1}$  ( $+UV$ ) (Figure 2B). This shows that UV-induced optical Marangoni flows at the drop center were more intense than naturally occurring concentration gradient-induced surface flows. These optical Marangoni flows resulted in a flow pattern inside the drop that transported particles to the substrate and accumulated them at and around the vertical of the irradiated area. We then utilized lower magnification imaging to characterize the deposition behavior at the whole drop level while keeping reduced evaporation conditions (Figure 2C). The developed flow was axisymmetric with two distinguishable regions: (i) a circulating flow pattern pointing toward the drop center and bringing particles down to the substrate surrounded by (ii) another circulating flow rotating in the same direction (Figure 2E). The central flow pattern is in agreement with the streak image analysis (Figure 2A) and is attributed to the optical Marangoni flows oriented toward the illuminated area. The surrounding flow is reminiscent of Marangoni eddies that develop at the contact line of evaporating drops containing surfactants, due to the concentration gradient in the direction of the contact line.<sup>38</sup> The boundary between these two flows generated a cylindrical volume where particles were trapped. Initially close to the drop edge, this trapping volume progressively shrank toward the drop center to reach a steady-state position where most particles had accumulated (Figure 2C and Supporting Information, Movie S3). Under normal evaporation conditions, although the outward convective flow tended to scatter the particles accumulated at the drop center toward the contact line

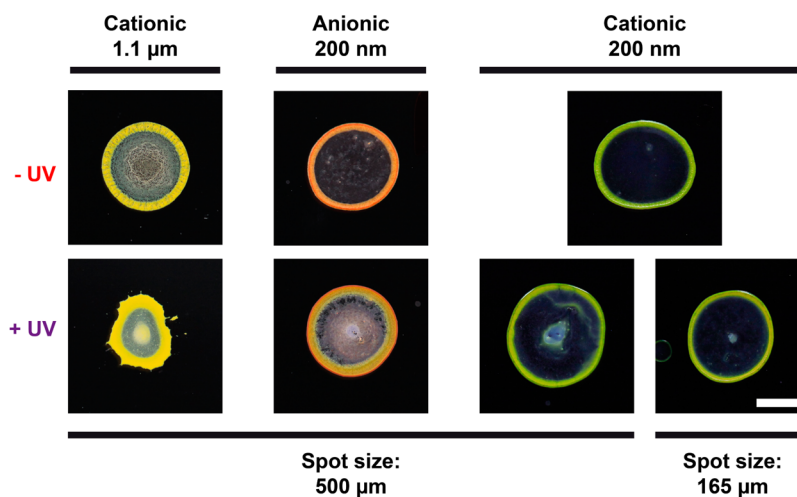


**Figure 4.** Versatile particle patterning. Real-color reflection images of deposits obtained without (top) or with (bottom) UV irradiation (fixed focused spot with a diameter of 500 or 165  $\mu\text{m}$ ) of a 7  $\mu\text{L}$  suspension colloidal drop containing 1.1  $\mu\text{m}$  diameter cationic ( $2 \text{ mg}\cdot\text{mL}^{-1}$ ), 200 nm diameter anionic ( $2 \text{ mg}\cdot\text{mL}^{-1}$ ) and 200 nm diameter cationic ( $4 \text{ mg}\cdot\text{mL}^{-1}$ ) particles with AzoTAB (10 mM). Light intensity was  $1.0 \times 10^3 \text{ W}\cdot\text{m}^{-2}$  (left, middle) and  $2.5 \times 10^2 \text{ W}\cdot\text{m}^{-2}$  (right). Scale bar is 2 mm.

(especially at the late stage of evaporation), most particles remained in the trapping volume defined by the flow boundary, resulting in a final deposit with a well-defined, circular shape (Figure 2D and Supporting Information, Movie S4). eOMA thus relies on light-driven Marangoni flows inducing a solutal flow pattern that efficiently combines with the outward evaporation-driven flow to deposit most of the particles at the illuminated area (Figure 2F).

To assess the flexibility of this new light-directed assembly strategy, we applied different in- and off-center light patterns (Figure 3). The first method was to apply a single UV spot (500  $\mu\text{m}$  diameter) at different positions during drop evaporation. UV was applied for 2 min at each position and this light pattern was repeated in a cyclic manner until complete drying. Following this way, we reproducibly obtained 2, 3, or 4 circular patches of particles, which were specifically deposited at each illuminated position (Figure 3A). Another method was to apply UV light through a photomask and defocus the beam to get the mask image projected on the drop surface. With this method, patterns with a controllable number of spots at predefined positions could also be obtained (Figure 3B) as well as more complex shapes such as lines or letters (Figure 3C). We noticed that applying intermittent UV illumination (e.g., 2 min on, 2 min off) provided patterns with better resolution and reproducibility than a continuous illumination (Supporting Information, Figure S2), mainly because of the increased occurrence of contact line depinning when complex light-induced flow patterns were generated continuously. It is worth mentioning that each deposited patch of particles was surrounded by a depletion zone where few particles were present. Timelapse observations confirmed that the deposition mechanism was mainly driven by the light-induced flow pattern inside the drop (Supporting Information, Figure S3 and movie S5). To our knowledge, this is the first time that such a spatial control over particle deposition can be obtained in individual sessile evaporating drops.

Because eOMA is based on flows rather than interactions, and therefore applicable in principle to any kind of particles, we challenged its versatility by applying it to suspensions of particles of different sizes and charges (Figure 4). Using single spot illumination on the center of the drop, the deposition of

cationic particles of similar size (amine-modified polystyrene, 1.1  $\mu\text{m}$  diameter) was successfully guided by light, even when partial depinning occurred (Figure 4 left). In the case of smaller particles (200 nm diameter), which led to marked ring patterns in the absence of irradiation, UV also directed the deposition of particles toward the irradiated area for both anionic (Figure 4 middle) and cationic (Figure 4 right) particles. Regardless of particle size and charge, the final particle pattern had a similar size when the light spot diameter and intensity were fixed. Interestingly, all other parameters being kept constant (including the light intensity, here  $2.5 \times 10^2 \text{ W}\cdot\text{m}^{-2}$ ), we found that the size of the particle patch was directly correlated to the size of the UV spot. For instance, a 3-fold decrease of the spot size led to a comparable reduction of the particle pattern diameter (Figure 4, right). All results described in Figures 3 and 4 thus show that eOMA can be used to direct the deposition of various kinds of particles into arbitrary predefined positions where the shape, size, and resolution of the resulting particle pattern are primarily dictated by the light pattern characteristics (static or dynamic, size, shape, intensity) rather than inherent particle properties (size and charge).

Finally, we tested the applicability of eOMA on complex formulations of unknown composition. We directly applied our method to actual coffee (instant coffee powder dissolved in tap water at a drinkable concentration). Without irradiation, the drop left a typical coffee-colored ring-shaped deposit after drying (Figure 5A top). However, it can be noticed that a small amount of materials was also deposited in the center of the drop, as seen in the profilometry analysis (Figure 5B, -UV), probably due to Marangoni flows toward the drop apex induced by the presence of surface active molecules in the coffee formulation and AzoTAB. Remarkably, when a circular UV spot was applied on the center of the coffee drop, a clear accumulation of brown colored material, mainly attributed to coffee particles, was observed in the dried pattern (Figure 5A bottom) and was confirmed by profilometry analysis (Figure 5B, +UV). This shows that the deposition of coffee particles during drop drying was successfully directed by light. Strikingly, more elaborate patterns could also be generated when the coffee drop was illuminated through a photomask during

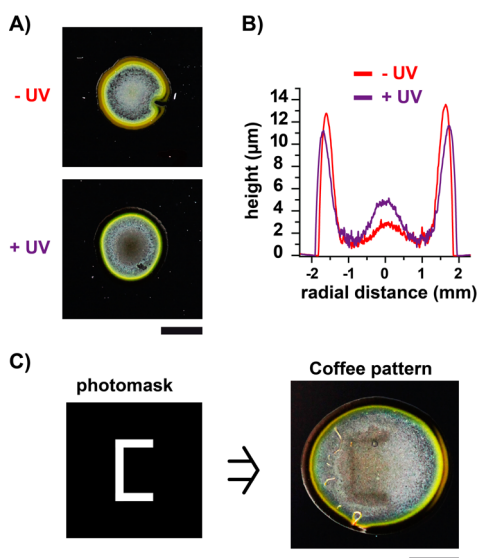


**Figure 5.** Particle patterning from real-world formulations (here, coffee) A-B) Real-color reflection images (A) and profilometry analysis (B) of deposits obtained without or with UV irradiation (fixed focused spot) of a 7  $\mu\text{L}$  coffee drop (instant commercial coffee, 5  $\text{mg}\cdot\text{mL}^{-1}$ ) with AzoTAB (10 mM). (C) Real-color reflection image (right) of deposit obtained with UV irradiation using a projected image through a photomask (left) on a 15  $\mu\text{L}$  coffee drop of the same composition. All scale bars are 2 mm.

drying, as demonstrated here by the specific deposition of coffee particles to form the letter “C” (Figure 5C).

In summary, we have described a novel flow-based, light-guided deposition method to organize particles on solid substrates regardless of their size or surface chemistry. This strategy is remarkable for its simplicity and versatility, making it suitable not only for model colloidal suspensions but also for complex, real-world formulations.

## ■ ASSOCIATED CONTENT

### Supporting Information

The Supporting Information is available free of charge on the ACS Publications website at DOI: 10.1021/acs.nanolett.5b04377.

Materials and methods, chemical structure of AzoTAB (Figure S1), effect of UV irradiation time (Figure S2); timelapse of patterning the letter “C” (Figure S3), and ledgers for Movies S1–S5 (PDF)

High-magnification observation of flows without (Movie S1) and with (Movie S2) UV irradiation, whole drop observation of flows with UV irradiation under reduced (Movie S3) and normal (Movie S4) evaporation conditions, and observation of an evaporating drop irradiated with a “C” light pattern (Movie S5) (ZIP)

## ■ AUTHOR INFORMATION

### Corresponding Author

\*(D.B.) Telephone: +33 1 4432 2405. E-mail: [damien.baigl@ens.fr](mailto:damien.baigl@ens.fr). Website: <http://www.baigllab.com/>.

### Author Contributions

These authors contributed equally. The manuscript was written through contributions of all authors. All authors have given approval to the final version of the manuscript.

## Funding

This work was supported by the European Research Council (ERC) [European Community’s Seventh Framework Programme (FP7/2007–2013)/ERC Grant Agreement No. 258782] and the Mairie de Paris [Emergence(s) 2012]. MA acknowledges funding from the European Commission (FP7-PEOPLE-2013-IEF/Project 624806 “DIOPTRA”).

## Notes

The authors declare no competing financial interest

## ■ ACKNOWLEDGMENTS

We thank Y. Chen and E. Aït-Yahiatène for experimental support.

## ■ REFERENCES

- (1) Xia, Y.; Gates, B.; Yin, Y.; Lu, Y. *Adv. Mater.* **2000**, *12*, 693–713.
- (2) Maier, S. A.; Brongersma, M. L.; Kik, P. G.; Meltzer, S.; Requicha, A. A. G.; Koel, B. E.; Atwater, H. A. *Adv. Mater.* **2003**, *13*, 1501–1505.
- (3) Duggal, R.; Hussain, F.; Pasquali, M. *Adv. Mater.* **2006**, *18*, 29–34.
- (4) Han, W.; Lin, Z. *Angew. Chem., Int. Ed.* **2012**, *51*, 1534–1546.
- (5) Zhang, Z.; Zhang, X.; Xin, Z.; Deng, M.; Wen, Y.; Song, Y. *Adv. Mater.* **2013**, *25*, 6714–6718.
- (6) Denkov, N. D.; Veleev, O. D.; Kralchevsky, P. A.; Ivanov, I. B.; Yoshimura, H.; Nagayama, K. *Nature* **1993**, *361*, 26–26.
- (7) Yin, Y.; Lu, Y.; Gates, B.; Xia, Y. *J. Am. Chem. Soc.* **2001**, *123*, 8718–8729.
- (8) Cui, Y.; Björk, M. T.; Liddle, J. A.; Sönnichsen, C.; Boussert, B.; Alivisatos, A. P. *Nano Lett.* **2004**, *4*, 1093–1098.
- (9) Vogel, N.; Retsch, M.; Fustin, C.-A.; del Campo, A.; Jonas, U. *Chem. Rev.* **2015**, *115*, 6265–6311.
- (10) Kraus, T.; Malaquin, L.; Schmid, H.; Riess, W.; Spencer, N. D.; Wolf, H. *Nat. Nanotechnol.* **2007**, *2*, 570–576.
- (11) Ueda, M.; Kim, H.-B.; Ichimura, K. *J. Mater. Chem.* **1994**, *4*, 883–889.
- (12) Klajn, R.; Wesson, P. J.; Bishop, K. J. M.; Grzybowski, B. A. *Angew. Chem., Int. Ed.* **2009**, *48*, 7035–7039.
- (13) Palacci, J.; Sacanna, S.; Steinberg, A. P.; Pine, D. J.; Chaikin, P. M. *Science* **2013**, *339*, 936–940.
- (14) Piech, M.; George, M. C.; Bell, N. S.; Braun, P. V. *Langmuir* **2006**, *22*, 1379–1382.
- (15) Georgiadis, A.; Routh, A. F.; Murray, M. W.; Keddie, J. L. *Soft Matter* **2011**, *7*, 11098–11102.
- (16) Vieyra Salas, J. A.; Van Der Veen, J. M.; Michels, J. J.; Darhuber, A. A. *J. Phys. Chem. C* **2012**, *116*, 12038–12047.
- (17) Harris, D. J.; Hu, H.; Conrad, J. C.; Lewis, J. A. *Phys. Rev. Lett.* **2007**, *98*, 148301.
- (18) Roy, B.; Arya, M.; Thomas, P.; Jürgschat, J. K.; Venkata Rao, K.; Banerjee, A.; Malla Reddy, C.; Roy, S. *Langmuir* **2013**, *29*, 14733–14742.
- (19) Kumar, A.; Chuang, H. S.; Wereley, S. T. *Langmuir* **2010**, *26*, 7656–7660.
- (20) Garnier, N.; Grigoriev, R. O.; Schatz, M. F. *Phys. Rev. Lett.* **2003**, *91*, 054501.
- (21) Vela, E.; Hafez, M.; Régner, S. *Int. J. Optomechatronics* **2009**, *3*, 289–302.
- (22) Deegan, R. D.; Bakajin, O.; Dupont, T. F.; Huber, G.; Nagel, S. R.; Witten, T. A. *Nature* **1997**, *389*, 827–829.
- (23) Larson, R. G. *Angew. Chem., Int. Ed.* **2012**, *51*, 2546–2548.
- (24) Kuang, M.; Wang, L.; Song, Y. *Adv. Mater.* **2014**, *26*, 6950–6958.
- (25) Anyfantakis, M.; Baigl, D. *ChemPhysChem* **2015**, *16*, 2726–2734.
- (26) Anyfantakis, M.; Geng, Z.; Morel, M.; Rudiuk, S.; Baigl, D. *Langmuir* **2015**, *31*, 4113–4120.
- (27) Anyfantakis, M.; Baigl, D. *Angew. Chem., Int. Ed.* **2014**, *53*, 14077–14081.

- (28) Diguët, A.; Guillermic, R. M.; Magome, N.; Saint-Jalmes, A.; Chen, Y.; Yoshikawa, K.; Baigl, D. *Angew. Chem., Int. Ed.* **2009**, *48*, 9281–9284.
- (29) Chevallier, E.; Mamane, A.; Stone, H. A.; Tribet, C.; Lequeux, F.; Monteux, C. *Soft Matter* **2011**, *7*, 7866–7874.
- (30) Venancio-Marques, A.; Barbaud, F.; Baigl, D. *J. Am. Chem. Soc.* **2013**, *135*, 3218–3223.
- (31) Baigl, D. *Lab Chip* **2012**, *12*, 3637–3653.
- (32) Varanakkottu, S. N.; George, S. D.; Baier, T.; Hardt, S.; Ewald, M.; Biesalski, M. *Angew. Chem., Int. Ed.* **2013**, *52*, 7291–7295.
- (33) Venancio-Marques, A.; Baigl, D. *Langmuir* **2014**, *30*, 4207–4212.
- (34) Diguët, A.; Mani, N. K.; Geoffroy, M.; Sollogoub, M.; Baigl, D. *Chem. - Eur. J.* **2010**, *16*, 11890–11896.
- (35) Larson, R. G. *AIChE J.* **2014**, *60*, 1538–1571.
- (36) Biswas, S. C.; Chattoraj, D. K. *Langmuir* **1997**, *13*, 4505–4511.
- (37) Bhardwaj, R.; Fang, X. H.; Somasundaran, P.; Attinger, D. *Langmuir* **2010**, *26*, 7833–7842.
- (38) Still, T.; Yunker, P. J.; Yodh, A. G. *Langmuir* **2012**, *28*, 4984–4988.